Analysis of the Tangjiaxi Landslide-generated Waves in Zhexi Reservoir, China, by a Granular Flow Coupling Model

Huang Bolin[1, 2]✉, Yin Yueping[3], Wang Shichang[2], Tan Jianmin[2], Liu Guangning[2]
1. China Three Gorges University, Yichang, China, 443002; 2. Wuhan Centre of China Geological Survey, Wuhan, China, 430205; 3. China Institute for Geo-Environment Monitoring, Beijing, China, 100081.
E-mail: bolinhuang@aliyun.com

Abstract: A rocky granular flow commonly is formed after the failure of rocky bank slopes. An impulse wave disaster may also be initiated if the rocky granular flow rushes into a river with a high velocity. Currently, the granular mass/water coupling study is an important trend in the field of landslide-induced impulse wave. In this paper, a full coupling numerical model for landslide-induced impulse wave is developed based on non-coherent granular flow equation, i.e. Mih equation. In this model, Mih equation for continuous non-coherent granular flow controls movements of sliding mass, two-phase flow equation regulates the interaction between sliding mass and water, and the Re-Normalisation Group (RNG) turbulence model governs the movement of water body. The proposed model is validated and applied for the 2014 Tangjiaxi landslide of Zhexi Reservoir located in Hunan Province, China, to analyze the characteristics of both landslide motion and its following impulse waves. On July 16, 2014, a rocky debris flow was formed after the failure of Tangjiaxi landslide, damming Tangjiaxi stream and causing an impulse wave disaster with three dead and nine missing bodies. Based on the full coupling numerical analysis, the granular flow impacts the water with a maximum velocity of about 22.5 m/s. Moreover, the propagation velocity of the generated waves reaches up to 12 m/s. The maximum calculated run-up of 21.8 m is close enough to the real value of 22.7 m. The predicted landslide final deposit and wave run-up heights are in a good agreement with the field survey data. These facts verify the ability of the proposed model for simulating the real impulse wave generated by rocky granular flow events.

Key words: granular flow; coupling model; Tangjiaxi landslide; impulse wave; dynamic process

1. Introduction

Impulse waves are usually generated in reservoirs, rivers, lakes, and seas as rock/soil masses impact water, resulting in huge economic losses and casualties (Wang et al. 1986; Fritz 2001; Scheffers and Kelletat 2003; Alvarez-Cedrón et al. 2009; Silvia et al. 2011; Huang et al. 2012). This fact urges people to pay attention to landslide-induced impulse wave which is an interdisciplinary study related to rock/soil mechanics and fluid mechanics. A large number of researches have been done on landslide-induced impulse wave including analytical, physical, and numerical methods. The analytical solutions are derived from extensive sources, such as experiment and empirical formulae, where their application scope is limited to their sources (Kamphuis et al. 1970; Ataie-Ashtiani et al. 2008; Wieland et al. 1999; Ursell et al. 1960; Fritz et al. 2002; Huber and Hager 1997; Heller 2007; Yin and Wang 2008). Due to the considered simplifications for analytical solutions, it is hard to have an overall grasp of the landslide-induced impulse wave disaster (Heller et al. 2009). The scaled physical experiment method can well reproduce or preview the dynamic process of landslide-induced impulse waves (Ball 1970; Davidson and Whalin 1974; Muller and Schurter 1993). However, it requires a large amount of data, time, and money, and occupies a big space (Huang et al.2014). However, the numerical analysis method can help us have a relatively comprehensive analysis of the landslide-induced impulse wave disaster; it has the advantages of being precise, economic and reasonable, as well as having highly visible results (Heller et al. 2009). Therefore, the numerical analysis method is an efficient tool in the study of landslide-induced impulse wave (Yavari-Ramshe and Ataie-Ashtiani, 2016).

Regarding the granular mass/water body coupling system, three major numerical simulation methods have been recently applied, such as a) single model, b) simplified model, and c) full coupling model (Yavari-Ramshe and Ataie-Ashtiani, 2016). Each model may apply a mesh-based (e.g. finite difference method (FDM), finite element method (FEM), finite volume method (FVM), boundary element methods (BEM), et al.), or a particle-based (smoothed particle hydrodynamic (SPH), material particle method (MPM), et al.) method (Yavari-Ramshe and Ataie-Ashtiani, 2016) for numerical discretization of its model equations. In the single simulation method for landslide-induced impulse wave, the phase of landslide movement and granular mass/water body interaction are regarded as the formation of initial impulse wave, and generally the motion of the sliding mass is considered to the motion of a point. Therefore, various kinematic formulas, such as Newton's laws of motion, are applied to calculate the motion of the sliding mass (Heller 2009; Huang et al. 2012, 2016). Then, various empirical or experimental formulas of landslide-induced impulse waves are adopted to calculate the characteristics of the initial impulse wave caused by the landslide (Walder et al. 2003; Tappin et al. 2008; Watts et al 2003; Ataie-Ashtiani and Malek Mohammadi 2007). With the initial impulse wave as the initial input or boundary condition, the numerical simulation singularly aims at calculating the spread and run-up of impulse waves. Some examples of these models are TUNAMI (Fumihiko et al. 2006), MOST (Titov and Gonzalez 1997), FUNWAVE (Joseph et al. 2003; Tappin et al. 2008), CLAWPACK (Randall 2006), etc. Their accuracy and application scope largely depend on the source models for initial impulse wave. Many scholars (Watts et al. 2003; Ataie-Ashtiani and Malek-Mohammadi 2008; Di Risio et al. 2011; Yin et al. 2015) have studied initial impulse wave models in different range of application and introduced a large number of source models.

The simplified simulation for landslide-induced impulse wave means to simplify landslide motion in calculation. Some landslides are simplified as rigid bodies whose motion is mainly described with Newton's law of motion under gravity, friction, coupled water resistance, etc. (Das et al., 2009; Basu et al., 2009; Huang et al., 2013). For example, Yin et al. (2014) simulated the motion of Qianjiangping landslide as a rigid rotator and calculated the impulse waves. Harbitz et al. (2014) simulated a rockslide with the volume of 5×10^7 m^3 at Åkerneset fjord, western Norway as a rigid sliding block. Such simplified methods can reveal the rules of how various dynamic models of a rigid body affect impulse waves (Yin et al., 2015). For some flow-liked slides or debris flow, simple fluids or grains are used to simulate large deformation in the process of the motion of landslide. For instance, Ren et al. (2006) simulated the motion of Xintan landslide by regarding it as some large grains which complies with Newton's laws of motion and the law of conservation of energy. Gabl et al. (2015) used fluid to simulate landslide occurred at hillsides and the following impulse waves. Abadie et al. (2010) adopted the multi-phase flow model to simulate landslide-induced impulse waves, as a Newtonian fluid simulating the landslide. In these researches, simple fluids or grains are used for simplified simulation and thus the effects of landslide deformation on landslide-induced impulse waves could be taken into consideration at least partly in calculation.

The full coupling model for landslide-induced impulse wave is a currently emerging method, which is booming recently. The full coupling model can have a relatively accurate description of the motion of sliding mass, interaction with water, and consequent impulse waves. Simplified models have obvious difficulties in achieving an accurate description of the landslide motion. Accordingly, numerical models which consider the rheological behavior of the sliding mass in their calculations have been recently applied more often. The most applied continuous rheological models so far includes Coulomb model, Herschel–Bulkley model, Bagnlod model and Bingham model (Shakeri Majd and Sanders 2014; Cremonesi et al. 2011; Yavari-Ramshe and Ataie-Ashtiani, 2016; Xing et al., 2016). Those that describe avalanche, landslide or debris flow motions in discontinuous medium models are mainly FEM-DEM model (Morris et al. 2006; Munjiza 2004; Li et al., 2015) and DEM model (Smilauer et al. 2010; Brennen 2005; Utili et al. 2014). For generation, propagation and run-up of impulse waves, technologies that can finely depict large free surface deformations, such as VOF or non-hydrostatic models (Yavari-Ramshe and Ataie-Ashtiani, 2016) are adopted. Crosta et al. (2013) used an ALE-FEM approach for a 2D/3D simulation of landslide and impulse wave. Glimsdal et al. (2013) developed a model for submarine landslide and tsunami, where the landslide motion was simulated as a deformable viscoplastic Bingham fluid. Zhao et al. (2015) used 3D DEM-CFD coupling method to simulate the motion of vajont landslide and the resulting impulse waves. By combined a landslide dynamic model and a tsunami model, Sassa (2016) presented an integrated numerical model simulating the complete evolution of a landslide-induced tsunami. This model was applied to the 1792 Unzen-Mayuyama mega slide and tsunami disaster analysis.

In this paper, a full coupling model is developed for landslide-induced impulse wave based on non-coherent granular flow equation. The continuous granular flow model of Mih (1999) is applied to simulate the motion process of the rocky granular flow after rockslide. Then, a two-phase flow model is adopted for granular mass / water interaction coupled calculation. Taking Tangjiaxi rockslide and the resulting impulse wave as a case, a numerical analysis for the whole process is done to study the motion of the granular flow, its accumulation process and consequent formation, propagation and run-up of impulse waves. Meanwhile, the validity of the full coupling model for landslide-induced impulse is checked.

2. Theory and Methodology

Rockslides can be characterized by a rapid evolution, up to a possible transition into a rock avalanche, which can be associated with an almost instantaneous collapse and spreading (Utili et al. 2014). The failure of a rocky slope is commonly followed by a high concentration and non-coherent rocky granular motion. A large amount of non-coherent coarse solid grains as well as relatively few fine grains are densely distributed in the granular flows. They flow, deposit or erode along their motion routes, which spread very long in distance generally (Crosta et al. 2001). Such flowing characteristics of motion can be described through both the continuous rheological model and the discontinuous model. The discontinuous model for particle flow simulation has a natural similarity. For the discontinuous method, grains are generally simplified to be sphere. These grains can interact with each other through well-defined microscopic contact models (Hertz 1882; Zhang and Whiten 1996; Johnson 1985) and with the fluid (e.g. water or air) by empirical correlations of fluid and solid interaction models. However, the discontinuous method means a large challenge for individual researchers. That is because even for a small rockslide, the simulation will require numerous cells and huge computational resources, hard to be processed by personal computers (Utili and Crosta 2011). Whereas the model based on continuous granular flow is free from this problem.

High concentration granular flow was studied by several researchers such as Bagnold (1954), Savage (1978), Hanes and Inman (1985), Wang and Campbell (1992), Iverson (1997) and Mih (1999). Some rheological models such as coulomb and Voellmy consider no viscosity or shear rate in their rheological formulations (Iverson, 1997). In this study, the present continuous granular flow model is built by using viscous fluid.

2.1 Governing equations of granular flow

Landslide rheology describes landslide motions with shear stress (τ) or shear rate (Pudasaini 2011). Shear stress of granular flow is generally far larger than the cohesive shear stress of fluids that carry a small amount of grains. Shear stress in high concentration non-cohesive granular flow (τ_g) consists of: (1) Impact among solid particles (τ_i); (2) Additional viscous shear stress due to the presence of solid particles (τ_v); and (3) Shear stress in the fluid (τ_f) (Mih 1999). It becomes negligible in solid-gas flow when the dynamic viscosity of the gas is small. At high concentrations the principal contribution to the shear stress arises from impact forces (i.e., collision) among grains. Secondly, in general, smaller contribution arises from the distributed solid affecting the fluid. Bagnold (1954) performed shear cell experiments with different approaches and showed that an equation for cohesionless materials describes the relationship between bulk intergranular normal and shear stresses even in collision-dominated flows.

Extensive work, beginning with the 1954 work of Bagnold (1954) has been summarized and further extended to a larger range of experimental conditions by Mih (1999). He described the shear stress of a granular flow as follow:

$$\tau_g = \tau_v + \tau_i = 7.8\mu \frac{\lambda^2}{1+\lambda}\frac{du}{dy} + \rho_s \frac{0.015}{1+0.5\rho/\rho_g}\frac{1+e}{(1-e)^{0.5}}(\lambda D\frac{du}{dy})^2 \qquad (1)$$

Here: μ and ρ are the continuous fluid viscosity and fluid density between granular (e.g. air or water), ρ_g is the granular density, *e* is the coefficient of restitution associated with grain impacts, *D* is the grain diameter, and *d* is a function of the maximum solid volume fraction. Physically, $\lambda = d / S$, where *S* is defined as the average distance between grain centers. *u* is the mean velocity of the granular flow, y is the distance along the direction vertical to the moving direction, *du/dy* is the mean velocity gradient of the granular mixture.

The equation contains fluid viscous and impact coefficients. The fluid viscous coefficient is a constant. The impact coefficient has been correlated to the properties of the solid and fluid. The equation agrees reasonably well with several sets of experiments by different investigators which cover a wide range of granular flows (Mih, 1999).

2.2 Granular flow/fluid interaction

The granular flow is treated as incompressible fluid when applied with the shear stress equation of Mih (1999). The coupling model of granular flow and water adopts two phase model with two incompressible fluids having different densities. Supposing the water has density ρ_1, the granular flow has density ρ_2. The volume a fraction of the water making up a mixture is denoted by *f*, and the volume fractions of the granular is denoted by 1-*f*. The momentum balance for the continuous phase of water is

$$\frac{\partial u_1}{\partial t}+u_1\cdot\nabla u_1=-\frac{1}{\rho_1}\nabla P+F+\frac{K}{f\rho_1}u_r \qquad (2)$$

While for the dispersed phase or the granular, it is

$$\frac{\partial u_2}{\partial t}+u_2\cdot\nabla u_2=-\frac{1}{\rho_2}\nabla P+F-\frac{K}{(1-f)\rho_2}u_r \qquad (3)$$

Where:

u_1 and u_2 represent the velocities of the continuous and dispersed phases, respectively; F is the body force; P is the pressure; K is a drag coefficient that relates to the interaction of the two phases; u_r is the relative velocity difference between the dispersed and continuous phases:

$$u_r=u_2-u_1 \qquad (4)$$

The volume-weighted average velocity $\bar{u}$ of a mixture is Eq. (5).

$$\bar{u}=fu_1+(1-f)u_2 \qquad (5)$$

The volume-weighted average velocity momentum conservation equation is Eq. (6).

$$\nabla\cdot\bar{u}=0 \qquad (6)$$

The drag per unit volume (K) is calculated by Eq. (7).

$$K=\frac{1}{2}A_2\rho_1\left(C_DU+12\frac{\mu_1}{\rho_1R_2}\right) \qquad (7)$$

Where:

A_2 is the cross sectional area per unit volume of the dispersed phase;

ρ_1 and μ_1 are the water density and dynamic viscosity;

C_D is the user-specified drag coefficient. It is a dimensionless quantity and is 0.5 for spheres.

R_2 is the average particle size of the granular.

2.3 Governing equations of fluid flow

RNG k-ε model is used to calculate the fluid motion when the granular flow enters the water. The RNG model applies statistical methods to the derivation of the average equations for turbulence quantities, such as turbulent kinetic energy and its dissipation rate. The RNG model uses equations similar to the ones for the k-ε model. However, equation constants are derived explicitly in the RNG model, and it takes turbulent vortex into account. Generally, the RNG model has a wider applicability than the standard k-ε model. The transport equation for K_T includes the convection and diffusion of the turbulent kinetic energy, the production of turbulent kinetic energy due to shearing and buoyancy effects, diffusion, and dissipation due to viscous losses within the turbulent eddies (Yakhot and Orszag 1986; Yakhot and Smith 1992). The transport equation for K_T is:

$$\frac{\partial k_T}{\partial t}+\frac{1}{V_F}\left\{uA_x\frac{\partial k_T}{\partial x}+vA_y\frac{\partial k_T}{\partial y}+wA_z\frac{\partial k_T}{\partial z}\right\}=P_T+G_T+Diff_{k_T}-\varepsilon_T \quad (8)$$

An additional transport equation is solved for the turbulent dissipation, ε_T:

$$\frac{\partial \varepsilon_T}{\partial t}+\frac{1}{V_F}\left\{uA_x\frac{\partial k_T}{\partial x}+vA_yR\frac{\partial k_T}{\partial y}+wA_z\frac{\partial k_T}{\partial z}\right\}=\frac{CDIS1\cdot\varepsilon_T}{k_T}(P_T+CDIS3\cdot G_T)+Diff_\varepsilon-CDIS2\frac{\varepsilon_T^2}{k_T} \quad (9)$$

In the RNG turbulence transport models, the kinematic turbulent viscosity V_T is computed from

$$v_T=CNU\frac{k_T^2}{\varepsilon_T}$$

The diffusion of dissipation, $Diff_\varepsilon$ is:

$$Diff_\varepsilon=\frac{1}{V_F}\left\{\frac{\partial}{\partial x}(v_\varepsilon A_x\frac{\partial \varepsilon_T}{\partial x})+R\frac{\partial}{\partial y}(v_\varepsilon A_yR\frac{\partial \varepsilon_T}{\partial y})+\frac{\partial}{\partial z}(v_\varepsilon A_z\frac{\partial \varepsilon_T}{\partial z})+\xi\frac{v_\varepsilon A_x\varepsilon_T}{x}\right\} \quad (10)$$

Where k_T is the turbulent kinetic energy, V_F is the fractional volume open to flow, A_x is the fractional area open to flow in the x direction, A_y and A_z are similar area fractions for the flow in the y and z directions, respectively. P_T is the turbulent kinetic energy production term, G_T is the buoyancy production term, ε_T is the turbulence dissipation term. In the RNG model, CDIS1, CDIS3, and CNU are dimensionless user-adjustable parameters that have 1.42, 0.2 and 0.085 defaults. CDIS2 is computed from the turbulent kinetic energy (K_T) and turbulent production (P_T) terms (Yakhot and Orszag 1986; Yakhot and Smith 1992).

In particular, the RNG model is known to describe low intensity turbulence flows and flows having strong shear regions more accurately. The RNG model selected has already been successfully used to simulate impulse wave generated by landslides (Serrano-Pacheco et al. 2009; Basu et al. 2009; Das et al. 2009; Choi et al. 2007).

3. Case Study

A full coupling numerical analysis model for landslide-induced impulse wave is built based on coupled control equations. The model can stimulate the landslide motion of non-coherent granular flow and the generation, propagation and run-up process of impulse waves. The Tangjiaxi landslide event in Zhexi Reservoir, Hunan, China, is simulated as an example to analyze the whole process of the landslide motion and the impulse wave.

3.1 Overview of Tangjiaxi landslide and impulse wave

At 7 AM on July 16, Tangjiaxi landslide occurred on the left bank of Tangjiaxi Stream, a tributary of Zhexi Reservoir. The impulse wave induced by Tangjiaxi landslide destroyed the nearby residential area. The landslide is 700 m far from the mainstream of Chanxi stream (tributary of Zi River), and 10.6 km and 11.2 km away from Tangyanguang landslide site and Zhexi Dam along the watercourse, respectively (Fig. 1). Zhexi Dam is located in midstream of Zi River in Anhua County, Yiyang City, Hunan Province, China, and 15 km away from the seat of Anhua County. Zhexi Hydroelectric Station, which began to impound in February 1961, is a large hydroelectric station. Tangyangguang landslide occurred on March 6, 1961. It is the first impulse wave disaster generated by landslide since the founding of the People's Republic of China. The huge wave generated by Tangyanguang landslide overtopped Zhexi Dam and killed 64 persons (Du 1988). The impulse wave disaster generated by landslide happened again in this reservoir, which drew more attention.

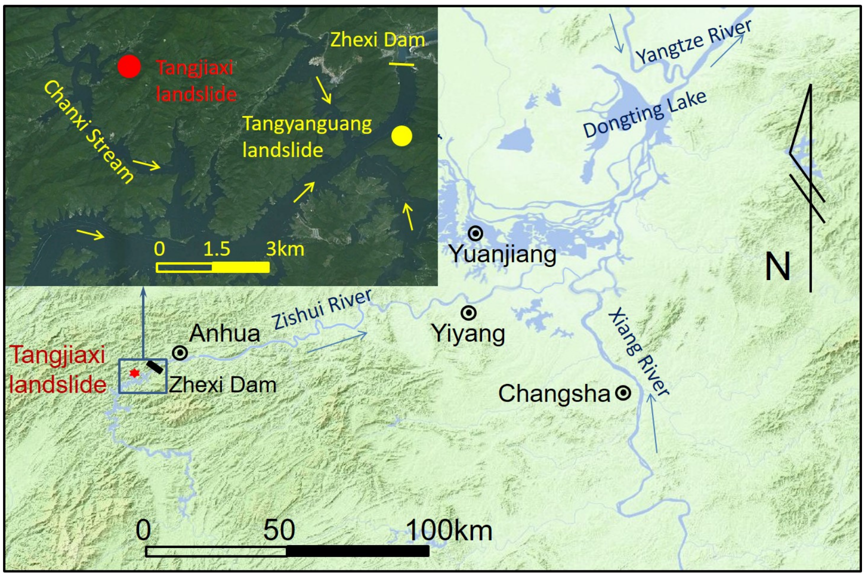

Fig. 1 The location of Tangjiaxi landslide in the Zhexi reservoir, Hunan Province, China

The landform of Tangjiaxi stream valley belongs to the type of medium gorge. The elevation of the highest mountain in this valley is 650 m, while the bottom elevation is 140-170 m generally. The overall flow direction of Tangjiaxi Stream is 245°, with a large gradient of about 1 km long. When water level elevation is 169.5 m, the stream is 2-100 m wide and 2-30 m deep. The original slope at valley bottom is about 25°~30°, and that at altitude above 200 m was 35°-45°. Generally, eluvial and diluvial deposit of 2-5 m thick was developed in the slope of the valley, with lush vegetable covered.

The rain continued for almost half a month from late June to early July in 2014. The daily rainfall was 98.5 mm around July 4. The Zhexi Reservoir was hit by rainstorm on July 13 again. The rainfall reached 102.5 mm on July 15 and seriously 239 mm on July 16 (Fig. 2). Rainfall increased the weight of sliding mass, formed greater underground water dynamic pressure, and decreased anti-sliding strength (Thomas 2003; Wang et al., 2004). Persistent rainfalls and heavy rainstorm directly triggered the failure of the landslide.

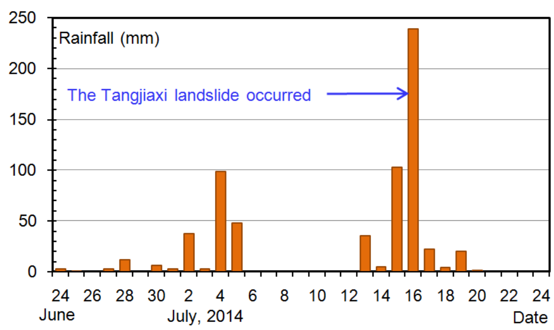

Fig. 2 Precipitation data monitored in Sifang village, 3.6 km from the landslide.

Fig. 3 Photo of first slide, taken by some local villager on July 16, 7 AM.

According to the description of many local survivors, the first slide occurred around 7 AM on July 16. Fig. 3 shows the scene of the first slide. Starting from the toe of the slope, the first slide was shallow soil slide which destroyed one of the three houses on the sliding mass. There was a short quiet period after the first slide. About 10:20 AM, rock blocks rolled down from the top of the slope and the global slide started. As soon as the landslide mass started to run out, rocks broke, crashed and rushed rumbly down to the slope foot, and houses were buried quickly. The mass impacted on Tangjiaxi stream at a high speed and induced huge waves, and the still water level was 169.5 m above sea level (asl.).

As shown in Fig. 4, the morphology of landslide scar was triangular in shape. The crown elevation of the landslide was about 315 m and the elevation of the outlet was about 155 m. The height difference was 160 m. At 26 m above the water surface, the landslide was 95 m wide, and at 56 m above the water surface, the landslide width reached 80 m. Much closer to the crown, the width of the landslide was smaller. The landslide was 15 m thick on average, with a total volume of 160,000 m^3, and main sliding direction was 320°.

Fig. 4 The scene of Tangjiaxi landslide, taken on July 23, 2014, when the water level was 167 m asl. The river was full of wood and debris, which were the destroyed building materials.

The underlying bedrock of Tangjiaxi Slope is Nantuo Formation (Z_n) and Guanyintian Formation of Sinian (Z_g) according to drilling reconnaissance and field survey. The lithology is grey-green till conglomerate and red metamorphosed quartz sandstone. The dip of schistosity of the rock mass is 300°-310° with the dip angle of 30°-40°. Two groups of faults with high dip angle are developed under the slope, which strike direction is nearly parallel to the valley. The fault belt is mylonite mainly (Fig. 5). Influenced by the fault, fissures are developed and there are mainly two groups of the structure planes: 1. fissures with a dip of 20°-30° and a dip angle of 60°-70°; 2.

fissures with a dip of 300°-320° and a dip angle of 65°-70°. Red or brown clay can be seen in some fissures. Two groups of structural planes and schistosity intersected mutually cataclasite structure rock mass were formed in Tangjiaxi slope.

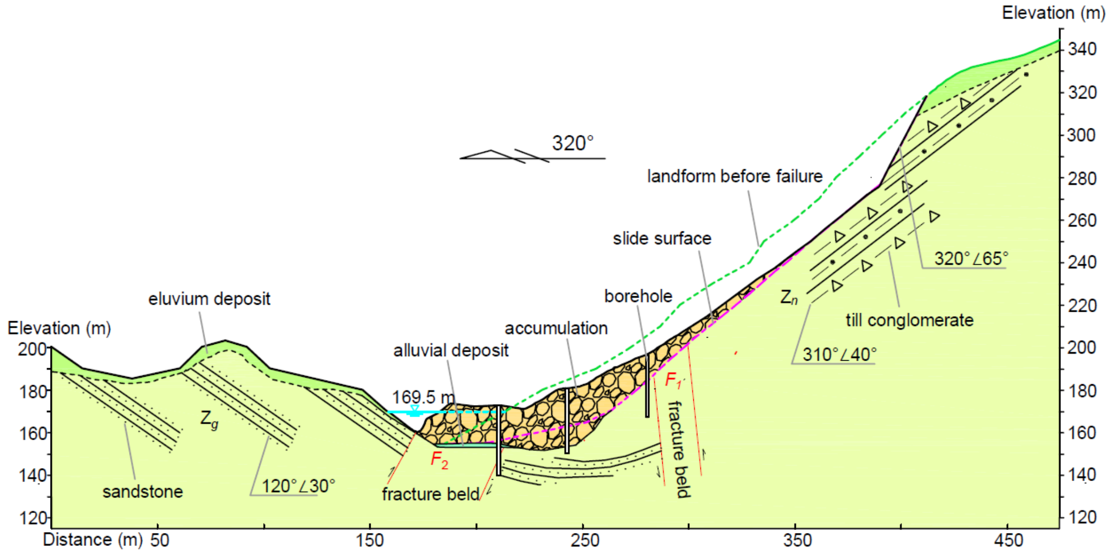

Fig. 5 Geological engineering section of Tangjiaxi landslide

After the landslide failed, cataclasite structure rock mass disintegrated quickly. The accumulation of sliding mass was mainly composed of rock blocks of different sizes. Medium and large rock blocks were mainly in the lower-middle part, with the maximum length of rock blocks of about 2.5 m. Rock blocks in the accumulation, having the shape of sharply angular with an average diameter of 30-40 cm, overhead stacking (Fig. 6). The few gravelly soils on the accumulation site were mainly distributed on the flanks of the landslide and at the front edge of accumulation fan. These soils were mainly derived from weathered layer and eluvial deposit of the original slope.

Fig. 6 accumulated blocks after Tangjiaxi landslide failure, taken in July 23, 2014.

Part of the sliding mass was accumulated in the watercourse and some stayed on the slope. The landslide dam raised the river bed and halted part of upstream water to form a small landslide lake.

The landslide dam was high in downstream and low in upstream, with bulge in the middle. Two terraces were formed on the vertical section. The dip angle of the deposits on the terrace was about 33°. The first slope terrace had an average elevation of about 180 m, 38 m long and 77 m wide, with a gradient of about 10°, while the second terrace had an average elevation of about 172.5 m, 75 m long and 98 m wide, with an average gradient of about 5-10°. The bulge was in the second terrace, with the top point of the elevation asl. of about 175.5 m. The river was broken by the second terrace of the landslide, which could be seen obviously in Fig. 7.

Fig. 7 Profile photo of Tangjiaxi Landslide, taken on July 23, 2014, when the water level is 167 m asl.

Witnesses described that it took only several seconds for the landslide to slide into the water and form the landslide dam. Calculated by 10 seconds for the sliding duration time, the landslide barycenter is about 70 m above still water surface and the sliding distance is about 120 m. It is estimated roughly that the biggest impact speed is about 24 m/s according to Newton's laws of motion. Huge impulse waves were triggered by the high-speed landslide. The impulse wave attacked the opposite bank, razed 6 houses to the ground, and cut trees to the root (Fig. 8 A). And then, the impulse wave flowed both upstream and downstream. The high-speed wave destroyed all houses (Fig. 8 B&D) and trees (Fig. 8 C) within its path. 9 houses were destroyed in this tsunamis event, 8 houses damaged and 121 persons of 17 families affected. The impulse wave caused three deaths, nine people missing, and eleven people wounded, six of them were badly hurt. Fortunately, owners of 5 destroyed houses went out for work and did not stay in the houses. Otherwise, the casualties would be more serious.

Though the watercourse in the landslide zone was only about 10m in average, the limited water gained great energy from the rock blocks granular mass at a high speed and formed huge impulse waves. As shown in the field survey, the maximum run-up was 22.7 m occurred in the opposite bank of the landslide; the upstream maximum run-up was 19.5 m occurred in a gully about 100 m upstream. At the downstream, with the increase of distance from the source of impulse wave, the run-up decayed. The maximum run-up at river mouth where Tangjiaxi stream flowed into the Chanxi stream was 1.8 m（Fig.8）. As the Tangjiaxi Stream flowed into the Chanxi Stream nearly vertically, the water surface suddenly became very wide, impulse wave decayed rapidly and no sign of impulse wave was seen on either bank of Chanxi stream.

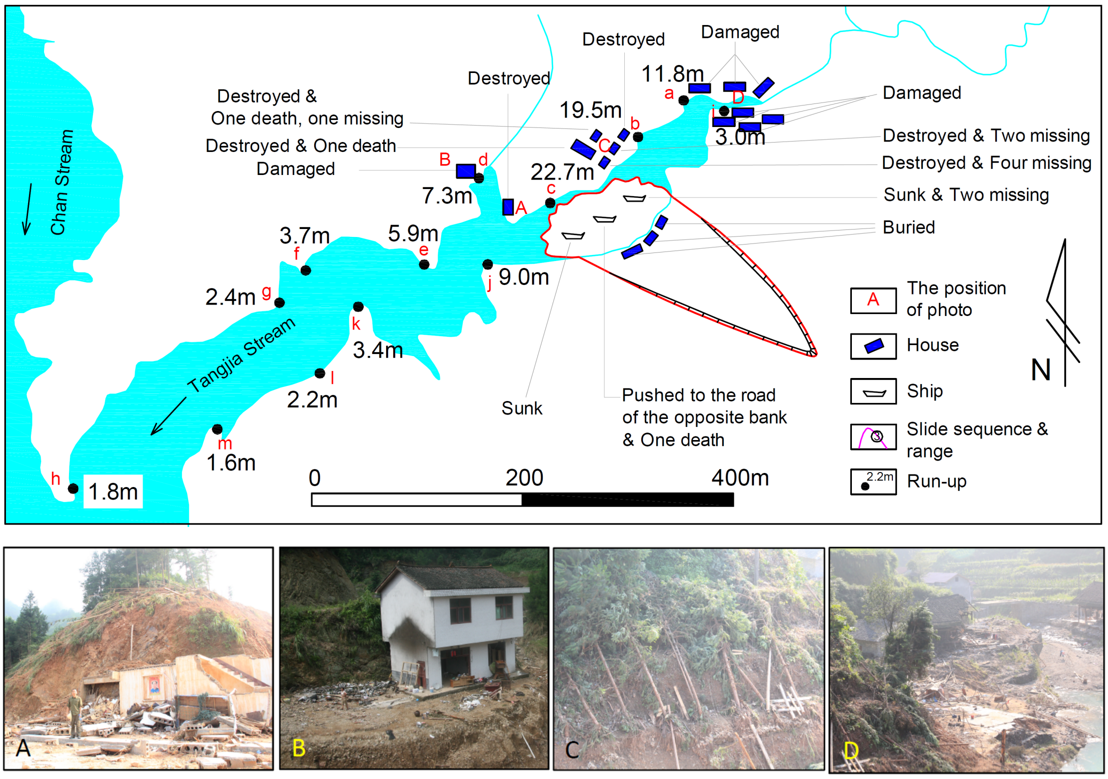

Fig. 8 The plot of run-up of the impulse wave generated by Tangjiaxi landslide, and the photos describe the scene of houses and trees damaged where marked by A, B, C and D in the upper map.

3.2 The granular flow coupling model

The computational domain which is considered to simulate the Tangjiaxi landslide-induced impulse wave by the full coupling numerical model covers the landforms of the valley where Tangjiaxi landslide occurred. The domain is 792 m long and 684 m wide including the valley source of Tangjiaxi stream at the tail of Zhexi Reservoir, with the lowest elevation of 140.0 m and the maximum mountain elevation of 740.2 m (Fig. 9). The digital elevation model of Tangjiaxi sliding mass is plotted based on the drilling survey and the topographic maps before and after the landslide, with a volume of about 158,000 m^3. As Tangjiaxi landslide failed under the condition of persistent rainstorm, the gaps between grains were basically filled with rainwater. Thus, the sliding material is can be supposed to be saturated. During the process of Tangjiaxi landslide motion, there were two distinct phases for the motion of rocky grains: start-up and moving phase and impact-stop phase in sequence. Impact in the first phase mainly occurred among grains and that in the second phase mainly between leading grains and the opposite bank. Therefore, two elastic restitution coefficients were adopted, and 0 was taken in the second phase when the leading granular flow impacts the bank. After trial calculation, 0.2 was taken in the first phase when the impact mainly occurred among grains, which makes the simulation results more realistic. Parameters required for granular flow motion calculation are as shown in Table 1. The parameters of density, average diameter and initial porosity of rock grains were determined through field survey and laboratory tests. Tangjiaxi sliding mass was in stationary initially and started moving under gravity. The granular flow moved and coupled with water after exposure to the river water.

Table 1 Main Parameters for Mih Equation Calculation

Parameter	Value	Parameter	Value

Fluid density	1000 kg/m^3	Grain restitution coefficient	0.2/0
Fluid viscosity	0.001pa.s	Average grain diameter	0.4 m
Grain density	2640 kg/m^3	Global vent coefficient	0.001

The water surface elevation in the model is 169.5 m asl., and the still water surface is the initial condition. Xmin surface is the zero flow boundary to ensure a constant water volume of Tangjiaxi stream. Zmax (water surface) is zero pressure boundary or free surface. Zmin surface, Xmax surface, Ymin surface and Ymax surface are all solid wall surfaces which is far away from the valley, so they are also zero flow boundaries. With the finite volume method with Euler algorithm adopted, there are 13,001,472 units in total in grid of 2 m × 2 m × 2 m. The simulation calculation of the numerical model lasts 30 s, After 6 s, the model come into the phase II as the leading granular flow impact the bank based on trial calculation.

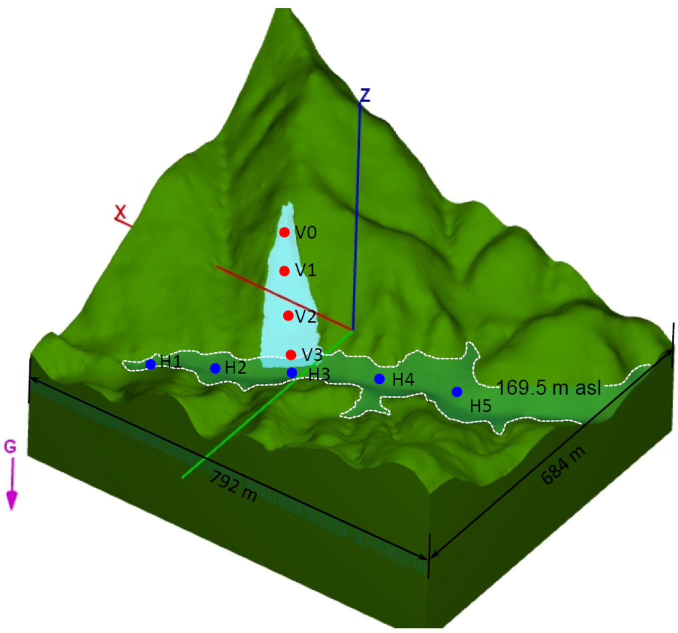

Fig. 9 Numerical model for Tangjiaxi landslide-induced impulse waves. Red points refer to the velocity monitoring points of the sliding mass motion and blue ones refer to the process monitoring points for water level.

3.3 Numerical results

In this simulation, the following aspects of the Tangjiaxi landslide event are analyzed: the motion process of the sliding mass and the process of impulse wave. And the model's validity was also checked through comparison with the field survey results.

3.3.1 Landslide movement process

The model analysis starts with the movement of the sliding mass. The depth-averaged velocity curves at different elevation points of the sliding mass show that the time of reaching to the maximum velocity is varied for different parts of the landslide. Most of the landslide parts reached to the maximum velocity before impacting the opposite valley at the 6th second. The maximum sliding velocity of the area at the rear edge (V0) was about 16.6 m/s; that at the middle of the sliding slope (V2) was about 30.9 m/s, possibly the maximum motion velocity of the sliding slope. V3 point located at the riverside with an elevation of 169.5 m, V3's velocity approximated to the speed at which the sliding mass impacted water, up to 22.5 m/s (Fig. 10). The value was equivalent to the maximum impact velocity estimated in field, which are 24 m/s. After the sliding mass impacted the opposite valley, the motion velocity of different parts of the sliding mass dropped sharply; when it went to about 10 s, the value at the middle and lower parts of the sliding mass was generally lower than 1 m/s, and that at the upper part was lower than 3 m/s. After 19 s, the velocity of the sliding mass was lower than 1 m/s in overall.

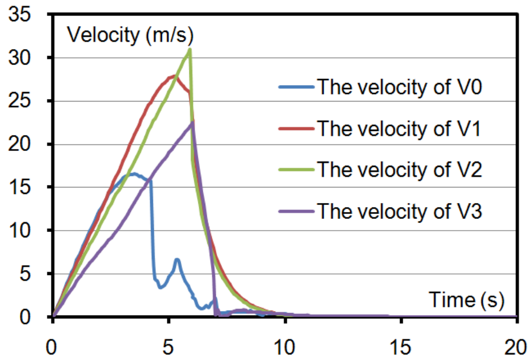

Fig. 10 Depth-averaged velocity process plot of monitoring points in the sliding mass. See Fig. 9 for positions of VO--V1.

Observed from the landslide configuration at different times, the motion of the sliding granular flow on land is generally within the scope of the sliding mass. After t=4.0 s, the sliding mass started to occupy the watercourse and extended to the upstream and the downstream, forming a fan shape (Fig. 11). It can be seen from the comparison with the final plane shape of the watercourse that numerical simulation results show a more ideal fan-shaped accumulation (Mohammed and Fritz 2005), and that the landslide dam shape formed in the numerical simulation differed from the actual situation (Fig. 12). This was possibly attributed to the presumption in the numerical model, i.e., the solid gains are ideally spherical, with a similar grain size.

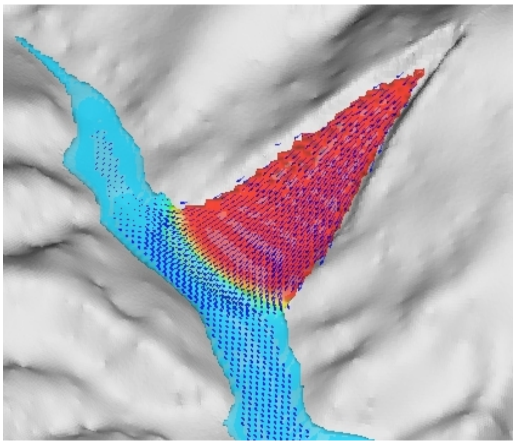

Fig. 11 Instantaneous state of Tangjiaxi landslide and river surface at t=4.0 s. In the figure, the red area is Tangjiaxi sliding mass, the cyan one is water, and the blue arrow is the motion direction of unit mass points.

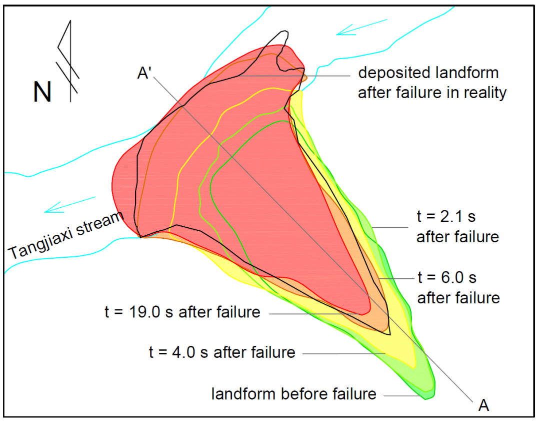

Fig. 12 Changes of plane shape after Tangjiaxi landslide failure

The depth profile of Section A-A' (Fig. 12) in Fig. 13 and the depth process of V0-V3 in Fig. 14

shows that the solid grains of the sliding mass gradually moved toward the valley and accumulated (Yavari-Ramshe et al. 2015). At t=2.1 s, substances in the sliding mass slid to the river bed. Substances with an elevation of over 200 m moved at high velocity, so sliding mass in the area started to get thinning. After 2.1 s, the sliding mass started to occupy the river bed in a large scale. At t=4.0 s, a small accumulated platform appeared in its early form in the valley, and kept moving to the opposite. At t=6.0 s, the slide front edge impacted the bank slope of the valley, when the landslide formed a large sliding dam in the valley and almost dammed the watercourse. At t=19.2 s, the landslide configuration was similar to that at t=6.0 s, and it remained unchanged forming a landslide dam with an average elevation of about 171 m. The actual average elevation of the landslide dam formed was about 172.5 m. From the section landform after the landslide deposited, we can see that the actual landform after landslide had an obvious two-step platform while the simulated result was only large one-step landslide platform, but their surface lines were similar.

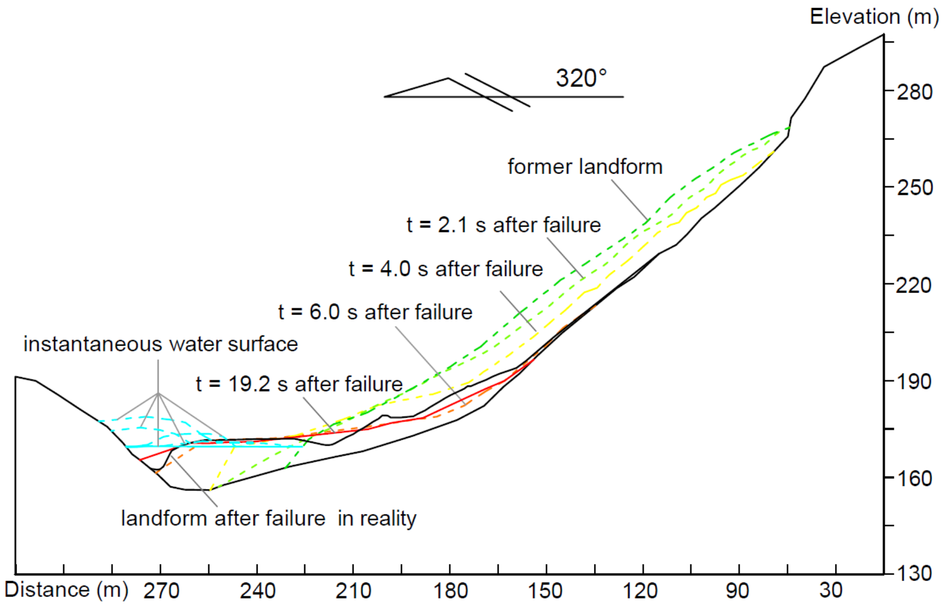

Fig. 13 A-A' Section form after Tangjiaxi landslide failure

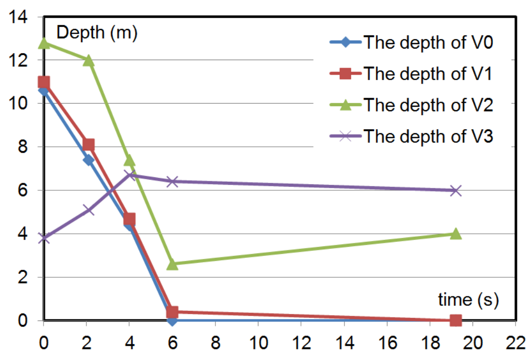

Fig. 14 Depth process plot of monitoring points in the sliding mass.

3.2 Process of impulse waves

The motion results of Tangjiaxi landslide simulated by the granular flow model show no significant differences from that in the field survey, basically reflecting the real motion process and characteristics of the landslide. Huge impulse wave was induced in stream due to the motion of granular flow.

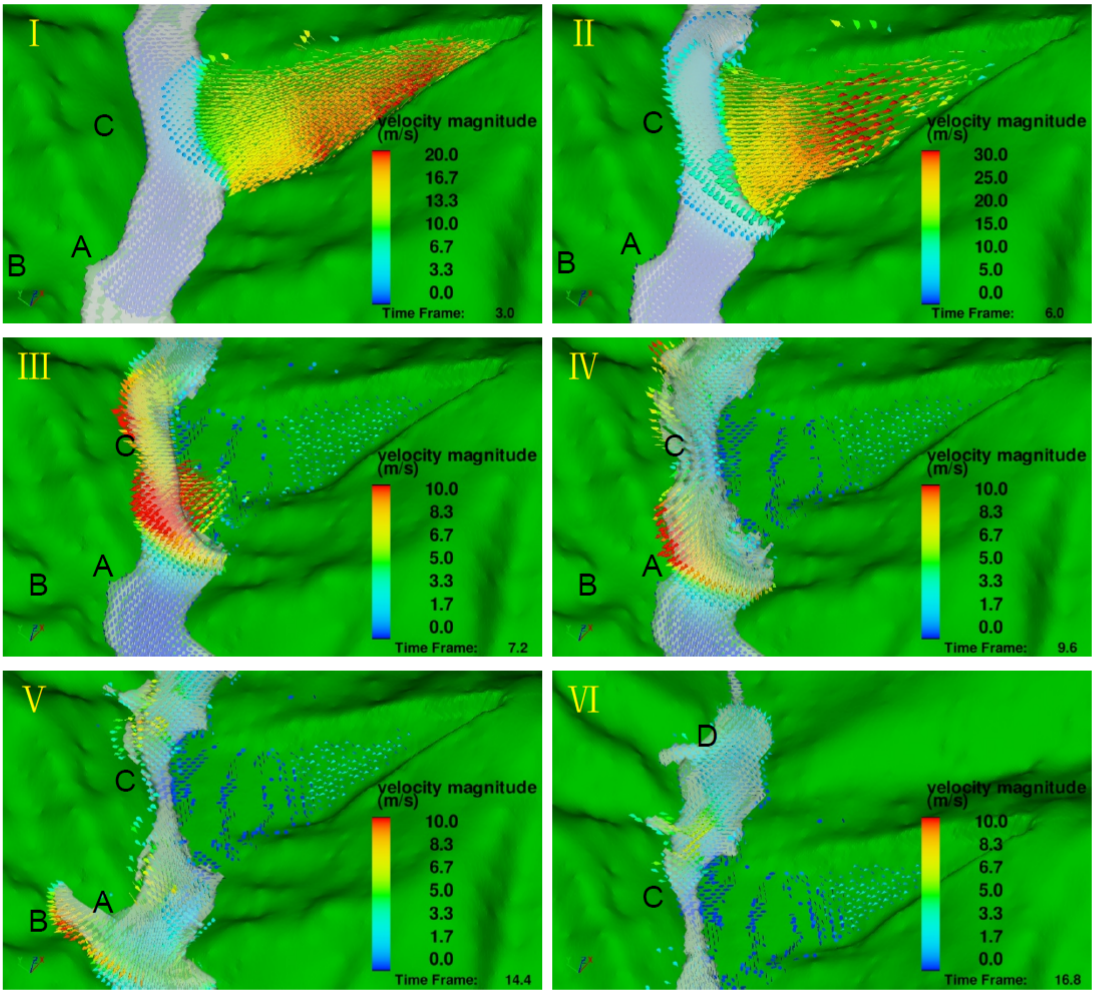

Fig. 15 Transient condition of river water and the vector diagram of mass. The arrow indicates the direction of movement, the color indicates the magnitudes shown in legend.

After the sliding mass occupied the watercourse, it pushed and supported the river water to move outwards and upwards in an arc shape (Fig. 13 and I in Fig. 15), similar to the forming of the impulse wave induced by Qianjiangping landslide. At t=6.0 s, an arc-shaped water wall formed on the river surface, about 10 m high and with the maximum water velocity of about 12.0 m/s, impacting the opposite and the upstream and the downstream (II in Fig. 15). The residential area in Area C was impacted firstly at the maximum impact velocity of 11.5 m/s (III in Fig. 15), resulting in a maximum run-up of 16.5 m in the area. At t=9.6 s, water reached to the ridge near A, with the maximum traveling velocity of 12.1 m/s (IV in Fig. 15). At t=11.1 s, water flowed over the ridge and impacted the houses of area A, with the maximum velocity of 11.6 m/s. At t=14.4 s, impulse waves started to impact houses in B, with the maximum velocity of about 7.0 m/s (V in Fig. 15). After 16.3 s, impulse waves spreading to the upstream reached the residential area in D, with the maximum water flow impact velocity dropping to 3.8 m/s (VI in Fig. 15). Based on the numerical results, it has taken about 20 sec since the landslide start moving until the impulse waves reached the first residential area. The impulse waves attacked at high velocity and caused serious house damages and heavy casualties in the area.

As it can be seen in Fig. 2, the Tangjiaxi valley is narrow. Therefore, it is hard to distinguish the generation, propagation and run-up phases of the impulse wave. Accordingly, this event was not a typical landslide-induced impulse waves. As it can be observed in the water level lines of various points in Tangjiaxi river surface in Fig. 16, there was only one large peak for the impulse waves, close to the landslide impact area (H3 in Fig. 16). Since the upstream of the landslide was quickly dammed after impulse waves arrived, water reaching the upstream failed to flow smoothly and therefore formed temporary upsurge in the upstream (Wang et al. 1986). The maximum upsurge in the upstream was up to 172.5 m (H2 in Fig. 16) and the upstream water level remained about 171. 6 m at 30 s. After a relatively large impulse wave, wave amplitude fluctuation in the landslide downstream watercourse attenuated (H4 in Fig. 16).

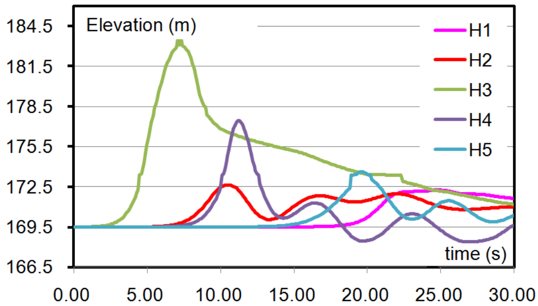

Fig. 16 Hydro Process Line of Various Points in Watercourse. See Fig. 9 for locations of H1--H5.

During the generation of this atypical landslide-induced impulse wave, it was hard to determine the maximum height of the first wave in the watercourse. The maximum propagating height of the wave in the peripheral watercourse of the landslide zone was about 8.0 m, located at the downstream of the landslide. The maximum run-up of the landslide was calculated to be 21.8 m at the opposite bank of the landslide; the run-up of this point in the field survey was 22.7 m. The slope at the opposite bank of the landslide was directly impacted by the impulse wave, with relatively higher run-up. In overall, the run-up was higher in the area where the landslide slid into water and gradually decreased in the periphery with the increase of distance. Table 2 shows the run-up at the bank surveyed in the field and corresponding calculated values. The correlation coefficient (R^2) of these two sets of data was 0.98, with an average error of 11%, indicating that calculated results adequately match with actual survey results, so the numerical model for landslide-induced impulse wave is reasonable and valid.

Table 2 The calculated and measured run-up values at different points

North Run-up (m)	Position	g	f	e	d	c	b	a
	Investigation	2.4	3.7	5.9	7.3	22.7	19.5	11.8
	Calculation	3.3	3.6	6.5	7.0	21.8	17.3	12.1
South Run-up (m)	Position	l	k	j	i			
	Investigation	2.2	3.4	9.0	3.0			
	Calculation	3.2	4.1	9.2	3.7			

The equations of Baglad and Mih were obtained from the experiments of sphere grains, and there is non-coherence among the grains. Although some parameters are taken by back analysis in the case, the dynamic capacity of sphere grains is bigger than grains with other sharp, which make the energy transferred to water higher. Meanwhile, in the actual situation, rock mass slides into water along with disintegrated. In the dynamic process, there should considerate general coherence to reflect these forces. Therefore, the run-up values simulated are larger than investigations in generally. Consideration of coherence and sharp of grain is a main modification direction for this granular flow coupling model, which might improve its realism for a wider range of applications.

4. Conclusion

In this paper, a full coupling numerical model for landslide-induced impulse wave was developed, The non-coherent granular flow model of Mih (1999) was used to simulate the dynamic characteristics of Tangjiaxi rockslide, and the two-phase flow model and RNG model were used to simulate the impulse waves while the granular flow impacted water.

Tangjiaxi rocky granular flow slid into the watercourse and then moved to the upstream and the downstream, forming a fan shape, and deposited to be a landslide dam in the valley, damming the watercourse. The sliding mass impacted water at the maximum velocity of 22.5 m/s, and at the moment the maximum celerity of wave was 12.1 m/s. It was an atypical impulse wave at the reach where the landslide slid into water, where the phases of generation, propagation and run-up of the impulse wave were hard to distinguish. The impulse wave induced by the landslide directly attacked the opposite residential area, with the maximum run-up of 21.8 m as calculated. Landslide dam formed hindered the downward flowing of water in the upstream, causing temporary upsurge.

Landslide dam configuration and impulse wave run-up calculated were well fit with the actual survey results. Therefore, the coupling model based on non-coherent Mih granular flow performed well in the whole-process analysis of Tangjiaxi landslide induced impulse wave. The framework of this coupling numerical model deserves more attention and further improvement.

Acknowledge:

This work was supported by National Natural Science Foundation of China (project ID: 41372321) and National Science and Technology Support (ID: 2012BAK10B01). Also, the authors would like to thank Mr. Xie from Tangjiaxi village who provide his photos and other useful information to us.

References:

Abadie S, Morichon D, Grilli S, Glockner S (2010) Numerical simulation of waves generated by landslide using a multiple-fluid Navier-Stokes model. Coast Eng, 57:779－794.

Alvarez–Cedrón C, Drempetic V (2009) Modeling of fast catastrophic landslides and impulse waves induced by them in fjords, lakes and reservoirs. Eng Geol 109:124–134

Ataie-Ashtiani B, Malek-Mohammadi S (2008) Mapping impulsive waves due to subaerial landslides into a dam reservoir: a case study of Shafa-Roud Dam. Dam Engineering, XVIII(3): 1-25.

Ataie–Ashtiani B, Nik–Khah A (2008) Impulsive waves caused by subaerial landslides. Environ Fluid Mech 8:263–280

Ataie-Ashtiani B，Malek Mohammadi S (2007) Near field amplitude of subaerial landslide generated waves in dam reservoirs. Dam Engineering, 17(4) : 197—222.

Bagnold RA (1954) Experiments on a gravity-free dispersion of large solid spheres in a Newtonian fluid under shear. Proc R Soc London, A225, 49-63.

Ball JW (1970) Hydraulic model studies, wave action generated by slides into Mica Reservoir. Technical report. Western Canada Hydraulic Laboratories, Vancouver, Canada

Basu D, Green S, Das K, Janetzke R, Stamatakos J (2009) Numerical simulation of surface waves generated by a sub-aerial landslide at Lituya Bay, Alaska. Proceedings of OMAE 2009, 28th international conference on ocean, offshore and arctic engineering, 1–14

Brennen CE (2005) Fundamentals of multiphase flow. Cambridge University Press, Cambridge.

Choi BH, Kim DC, Pelinovsky E, Woo SB (2007) Three--dimensional simulation of tsunami run ‑ up around conical island. Coast Eng 54:618–629

Cremonesi M, Frangi A, Perego U (2011) A Lagrangian finite element approach for the simulation of water-waves induced by landslides. Comput Struct 89:1086 ‑ 1093.

Crosta GB, Calvetti F, Imposimato S, Roddeman D, Frattini P, Agliardi F (2001) Granular Flow and Numerical Modelling of Landslides. Debrisfall Assessment in Mountain Catchments for Local End-users. Technique Report.

Crosta Giovanni B., Imposimato Silvia, Roddeman Dennis (2013) Monitoring and modelling of rock slides and rock avalanches. Italian Journal of Engineering Geology and Environment, 6: 3-14.

Das K, Janetzke R, Basu D, Green S, Stamatakos J (2009) Numerical simulations of tsunami wave generation by submarine and aerial landslides using RANS and SPH models. Proceedings of OMAE 2009, 28th international conference on ocean, offshore and arctic engineering. 1–14

Davidson DD, Whalin RW (1974) Potential landslide-generated water waves, Libby Dam and Lake Koocanusa, Montana. Technical report. Waterways Experiment Station of U.S. Army Corps of Engineers, Vicksburg

Davies DR, Wilson CR, Kramer SC (2011) Fluidity: a fully unstructured anisotropic adaptive mesh computational modeling framework for geodynamics. Geochemistry, Geophysics, Geosystems, AGU and Geomechanical Society 12(6), 20 pp. doi: 10.1029/2011GC003551

Du Bohui (1988) Tangyanguang landslide of Zhexi Reservoir: The first large-scale landslide occurred at early stage of impoundment in China. Proceedings of the 2nd Symposium on Rock & Soil and Engineering of China, Beijing: 918~922. (In Chinese)

Fritz HM (2002) Initial phase of landslide generated impulse waves. Thesis for the Ph.D, Zürich University

Fritz HM, Hager WH, Minor HE (2001) Lituya Bay case: rockslide impact and wave run–up. Sci Tsunami Hazards 19(1):3–22

Fumihiko Imamura, Ahmet Cevdet Yalciner, Gulizar Ozyurt (2006). Tsunami Modelling Manual. http://www.tsunami.civil.tohoku.

Gabl R, Seibl J, Gems B, and Aufleger M (2015) 3-D-numerical approach to simulate an avalanche impact into a reservoir. Nat. Hazards Earth Syst Sci Discuss, 3, 4121-4157.

Glimsdal S, L'Heureus JS, Harbitz CB, Pedersen GK (2013) Modelling of the 1888 Landslide Tsunami, Trondheim, Norway. Proc. the Second World Landslide Forum "Landslide Science and Practice", Springer, 5: 73-79.

Hanes DM and Inman DL (1985) Observations of rapidly flowing granular-fluid mixture. J Fluid Mechanics, 150, 357-380.

Harbitz CB, Glimsdal S, Løvholt F, Kveldsvik V, Pedersen GK, Jensen A (2014) Rockslide tsunamis in complex fjords: from an unstable rock slope at Åkerneset to tsunami risk in western Norway. Coast Eng 88:101 - 122. doi:10.1016/j.coastaleng.2014.02.003

Heller V (2007) Landslide generated impulse waves: prediction of near field characteristics. Thesis for the Ph.D Zürich University

Heller V, Hager WH, Minor HE (2009) landslide generated impulse wawes in reservoirs: basics and computation. Technical report. VAW, ETH Zurich

Hertz H (1882) Uber die beruhrung fester elastischer Korper. Journal fur die Reine und Angewandte Mathematik. 29:156–171

Huang BL, Yin YP, Liu GN, Wang SC, Chen XT, Huo ZT (2012) Analysis of waves generated by Gongjiafang landslide in Wu Gorge, Three Gorges Reservoir, on November 23, 2008. Landslides. doi:10.1007/s10346-012-0331-y.

Huang Bolin, Wang Shichang, Yin Yueping, Liu Guangning, Chen Xiaoting (2013) Fluid-solid coupling kinetic analysis on impulsive wave generated by rockfall. Journal of Jilin University (Earth Science Edition), 43(6): 1936-1942.

Huang Bolin, Yin Yueping, Du Chunlan (2016) Risk management study on impulse waves generated by Hongyanzi landslide in Three Gorges Reservoir of China on June 24, 2015. Landslide, 10.1007/s10346-016-0702-x

Huang Bolin, Yin Yueping, Wang Shichang, Chen Xiaoting, Liu Guanglin, Jiang Zhibing, Liu Junzhe (2014) A physical similarity model of an impulsive wave generated by Gongjiafang landslide in Three Gorges Reservoir, China. Landslides, 11:513–525

Huber A, Hager WH (1997) Forecasting impulse waves in reservoirs. Proc. 19th Congres Des Grands Barrages. ICOLD 31:993–1005

Iverson RM, Reid ME, Lahusen RG (1997) Debris-flow mobilization from landslides. Ann Rev Earth Planet Sci, 25:85-138.

Johnson KL (1985) Contact mechanics. Cambridge University Press, Cambridge

Joseph S. Walder, Philip Watts, Oscar E. Sorensen, Kenneth Janssen (2003) Tsunamis generated by subaerial mass flows. Journal of Geophysical research, 18(B5):2236-2255.

Kamphuis JW, Bowering RJ (1970) Impulse waves generated by landslides. Proc. 12th Coastal Engineering Conference, Washington D.C, New York, 1:575–588

Li SH,Tang DH,Wang Jie (2015) A two-scale contact model for collisions between blocks in CDEM. Science China(Technological Sciences), 09:1596-1603.

Mih W C (1999) High concentration granular shear flow. Journal of Hydraulic Research, 37(2): 229-248

Mohammed F and Fritz HM (2005) Experiments on Tsunamis Generated by 3D Granular Landslides. Submarine Mass Movements and Their Consequences (Mosher D C eds.), Advances in Natural and Technological Hazards Research, 28, 705-720.

Morris JP, Rubin MB, Block GI, et al.(2006) Simulations of fracture and fragmentation of geologic materials using combined FEM/DEM analysis. Int J Impact Eng, 33: 463–473

Muller D, Schurter M (1993) Impulse waves generated by an artificially induced rockfall in a Swiss lake. Proc. 25th IAHR Congress 4: 209–216

Munjiza A (2004) The Combined Finite-Discrete Element Method. Chichester: Wiley.

Pudasaini SP (2011) Some exact solutions for debris and avalanche flows. Phys Fluids 23(4):043301. doi:10.1063/1.3570532

Randall JL (2006) CLAWPACK Version 4.3 User's Guide. University of Washington. http://www.amath.washington.edu/~claw/.

Ren KJ， Jin F， Xu QQ (2006) Vertical Two-Dimensional Numerical Simulation for Landslide-Generated Waves. Journal of Yangtze River Scientific Research Institute, 2006, 23(2) : 1—4 (in Chinese)

Sassa Kyoji, Dang Khang, Yanagisawa Hideaki, He Bin (2016) A new landslide-induced tsunami simulation model and its application to the 1792 Unzen-Mayuyama landslide-and-tsunami distaster. Landslides, Doi 10.1007/s10346-016-0691-9

Savage SB (1978) Experiments of shear flows of cohesionless granular materials. Proc U.S.-Japan Seminar on Continuum Mech and Stat Approaches in mechanics of granular materials. S C Cowin and M Satake, Eds. Gakujutsu Bunken Fukykai, Tokyo, Japan, 241-254.

Scheffers A, Kelletat D (2003) Sedimentologic and geomorphologic tsunami imprints worldwide - a review. Earth Sci Rev 63:83 – 92. doi:10.1016/S0012-8252(03)00018-7

Serrano-Pacheco A, Murillo J, Garcı´a-Navarro P (2009) A finite volume method for the simulation of the waves generated by landslides. J Hydrol 373:273–289

Shakeri Majd M, Sanders BF (2014) The LHLLC scheme for two-layer and two-phase transcritical flows over a mobile bed with avalanching, wetting and drying. Adv Water Resour 67:16 – 31.

Silvia B, Marco P (2011) Shallow water numerical model of the wave generated by the Vajont landslide. Environ Model Softw 26:406–418

Smilauer ECV,Chareyre B, Dorofeenko S, Duriez J, Gladky A, Kozicki J, Modenese C, Scholtes L, Sibille L, Stransky J, Thoeni K (2010) Yade Documentation. http://yade-dem.org/doc/2010.

Tappin DR, Watts P, Grilli ST (2008) The Papua New Guinea tsunami of July 17, 1998: Anatomy of a catastrophic event. Nat. Haz. and Earth Sys. Sci., NHESS, 8, 243-266.

Thomas Glade (2003) Landslide occurrence as a response to land use change: a review of evidence from New Zealand. Catena, 51 (3–4): 297–314.

Titov VV, Gonzalez FI (1997) Implementation and Testing of the Method of Splitting Tsunami (MOST) Model. NOAA Technical Memorandum ERL PMEL-112.

Ursell F, Dean RG, Yu YS (1960) Forced small amplitude water waves: a comparison of theory and experiment. J Fluid Mech 7:3–52

Utili S, Crosta GB (2011) Modeling the evolution of natural cliffs subject to weathering: 2. Discrete element approach. J Geophys Res Earth Surf 116(F1):F01017

Utili S, Zhao T, Houlsby GT (2014) 3D DEM investigation of granular column collapse: evaluation of debris motion and its destructive power. Eng Geol 186:3–16

Wang D and Campbell C (1992) Reynolds analogy for a shearing granular material. J Fluid Mechanics, 244,527-546.

Wang DY, Liu SK (1986) Xintan landslide impulsive wave survey in June of 1985. Yangtze River 10:24–27

Wang Fa-Wu, Zhang Ye-Ming, Huo Zhi-Tao, Tatsunori Matsumoto, Bo-Lin Huang (2004) The July 14, 2003 Qianjiangping landslide, Three Gorges Reservoir, China. Landslides, 1: 157-162.

Watts P, Grilli ST, Kirby JT et al (2003) Landslide tsunami case studies using a Boussinesq model and a fully nonlinear tsunami generation model. Nat Hazards Earth Syst Sci 3:391–402

Wieland M, Gray JM, Hutter K (1999) Channelized free-surface flow of cohesionless granular avalanches in a chute with shallow lateral curvature. J Fluid Mech 392:73–100

Xing Aiguo, Xu Qiang, Zhu Yaoqiang, Zhu Jiliang, Liang Yao (2016) The August 27, 2014, rock avalanche and related impulse water waves in Fuquan, Guizhou, China. Landslides, 13: 411-422.

Yakhot Victor and Orszag Steven A (1986) Orszag. Renormalization group analysis of turbulence I. basic theory. J. Sci. Comput., 1(1):3–51

Yakhot Victor and Smith Leslie M (1992) The renormalization group, the e-expansion and derivation of turbulence models. J. Sci. Comput., 7(1):35–61

Yavari-Ramshe S, Ataie-Ashtiani B, Sanders B F (2015) A robust finite volume model to simulate granular flows. Computers & Geotechnics, 66:96-112.

Yavari-Ramshe S. and Ataie-Ashtiani B. (2016) Numerical modeling of subaerial and submarine landslide-generated tsunami waves--recent advances and future challenges. Landslides, Doi 10.1007/s10346-016-0734-2

Yin KL, Du J, Wang Y (2008) Analysis of surge triggered by Dayantang landslide in Shuibuya Reservoir of Qingjiang River. Chin J Rock Soil Mech 29(12):3266–3270

Yin Yueping, Huang Bolin, Chen Xiaoting, Liu Guangning, Wang Shichang (2015) Numerical analysis on wave generated by the Qianjiangping landslide in Three Gorges Reservoir, China. Landslides, 12: 355-364.

Yin Yueping, Huang Bolin, Liu Guangning, Wang Shichang (2015) Potential risk analysis on a Jianchuandong dangerous rockmass-generated impulse wave in the Three Gorges Reservoir, China. Environ Earth Sci, 74: 2595-2607

Yin Yueping, Huang Bolin, Wang Shichagn Li Jinhe (2015) Potential for a Ganhaizi landslide-generated surge in Xiluodu Reservoir, Jinsha River, China. Environ Earth Sci, 73: 3187-3196.

Zhang D, Whiten WJ (1996) The calculation of contact forces between particles using spring and damping models. Powder Technol 88(1):59–64

zhao T, Utili S, Crosta G B (2015) Rockslide and impulse wave modelling in the Vajont Reservoir by DEM-CFD Analyses. Rock Mech Rock Eng, DOI 10.1007/s00603-015-0731-0